Inorganic Chemistry

ARTICLE

pubs.acs.org/IC

Cooperative Spin Transition in the Two-Dimensional Coordination Polymer [Fe(4,4′-bipyridine)$_2$(NCX)$_2$]·4CHCl$_3$ (X = S, Se)

Christopher J. Adams,*[,†] M. Carmen Muñoz,[‡] Rachel E. Waddington,[†] and José Antonio Real*[,§]

[†]School of Chemistry, University of Bristol, Bristol BS8 1TS, U.K.

[‡]Departament de Física Aplicada, Universitat Politècnica de València, Cami de Vera s/n, E-46022, Valencia, Spain.

[§]Instituto de Ciencia Molecular, Universidad de Valencia, C/Catedràtico José Beltrán Martínez, 2, 46980 Paterna, Valencia, Spain

Supporting Information

ABSTRACT: Two new isostructural two-dimensional (2D) coordination polymers exhibiting spin crossover (SCO) behavior of formulation [Fe(4,4′-bipy)$_2$(NCX)$_2$]·4CHCl$_3$ (4,4′-bipy = 4,4′-bipyridine; X = S [**1·4CHCl$_3$**], Se [**2·4CHCl$_3$**]) have been synthesized and characterized, and both undergo cooperative spin transitions (ST). For **1·4CHCl$_3$** the ST takes place in two steps with critical temperatures of T_{c1}^{down} = 143.1 K, T_{c2}^{down} = 91.2 K, T_{c1}^{up} = 150.7 K, and T_{c2}^{up} = 112.2 K. **2·4CHCl$_3$** displays half ST characterized by T_c^{down} = 161.7 K and T_c^{up} = 168.3 K. The average enthalpy and entropy variations and cooperativity parameters associated with the ST have been estimated to be ΔH_1^{av} = 5.18 kJ mol^{-1}, ΔS_1^{av} = 35 J K^{-1} mol^{-1}, and Γ_1 = 2.8 kJ mol^{-1} and ΔH_2^{av} = 3.55 kJ mol^{-1}, ΔS_2^{av} = 35 J K^{-1} mol^{-1}, and Γ_2 = 2.6 kJ mol^{-1} for **1·4CHCl$_3$**, and ΔH^{av} = 6.25 kJ mol^{-1}, ΔS^{av} = 38.1 J K^{-1} mol^{-1}, and Γ = 3.2 kJ mol^{-1} for **2·4CHCl$_3$**. At $T > [T_{c1}$ (**1·4CHCl$_3$**); T_c (**2·4CHCl$_3$**)], both compounds are in the space group $P2/c$ while at $T < [T_{c1}$ (**1·4CHCl$_3$**); T_c (**2·4CHCl$_3$**)] they change to the $C2/c$ space group and display an ordered checkerboard-like arrangement of iron(II) sites where the high- and low-spin states coexist at 50%.

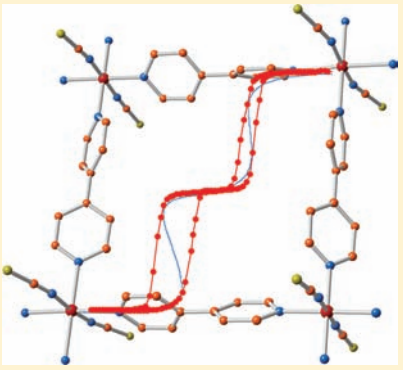

INTRODUCTION

Interest is currently growing in the field of six-coordinated iron(II) compounds that show spin-crossover (SCO) properties. They switch between the high-spin (HS) state $t_{2g}^4e_g^2$ (S = 2) and the low-spin $t_{2g}^6e_g^0$ (S = 0) (LS) state in a reversible and controllable way in response to external stimuli (usually temperature, pressure, and/or light). Because of the antibonding nature of the e_g orbitals, their population-depopulation provoke drastic structural changes at the coordination sphere of iron(II). In the solid state these structural changes may be transmitted cooperatively from one site to another by elastic interactions. In the case of strong coupling between the SCO sites, the magnetic, optical, and dielectric properties of the material change abruptly and, in the most interesting cases, this abrupt change is accompanied by thermo- and/or piezo-hysteretic behavior conferring upon the material a bistable nature, which could ultimately be used for the construction of sensory and memory devices.[1,2]

Extended one-, two-, and three-dimensional (1D, 2D, 3D) spin crossover coordination polymers (SCO-CPs) have become one important source of SCO compounds. Since the first reported examples of SCO-CPs, belonging to the two related series of 1D triazole-based complexes [Fe(Htrz)$_2$(trz)](BF$_4$)[3] and [Fe(4-Rtrz)$_2$](Anion)$_2$,[4] an important variety of 1D, 2D, and 3D SCO-CPs derived from triazoles,[5] tetrazoles,[6] pyridine-like bridging ligands,[7] and anionic bridges such as cyanometallates,[8] dicyanamide,[9] or polynitriles[10] have been reported. Within these SCO-CPs, 2D compounds which may be generically formulated {Fe(L)$_2$(NCX)$_2$}·nSolv have been important in the search for new SCO-CPs, as they display a variety of SCO behaviors, interesting network structures and properties. Typically such coordination networks contain iron(II) centers surrounded by six N-donor ligands in an octahedral configuration, with monodentate pseudohalide ligands in the two axial positions and bis-monodentate pyridine-like bridging ligands (L) in the four equatorial positions, which allows the coordination network to form a (4,4) grid. Such a grid contains square windows whose size depends on the length of L. For small-medium L lengths the crystal packing is made up of a simple parallel stacking of the grids as described for the archetypal compound {Fe(btr)$_2$(NCX)$_2$} (X = S,[11] Se;[12] btr = 4,4′-bis-1,2,4-triazole). However, for large enough bridging ligands the network may be doubly or triply interpenetrated; networks of this kind include {Fe(bpb)$_2$(NCS)$_2$} (bpb = 1,4-bis(pyridyl)butadiyne),[13] {Fe(tvp)$_2$(NCS)$_2$} (tvp = 1,2-bis(pyridyl)ethene),[14] {Fe (bpbd)$_2$(NCS)$_2$} (bpbd = 2,3-bis(4′-pyridyl)-2,3-butanediol)[15,16] and {[Fe(azpy)$_2$(NCS)$_2$} (azpy = 4,4′-azopyridine).[17,18] In many cases these networks clathrate solvent molecules, which have a profound effect on their SCO behavior. This can be in the form of switching the SCO activity on and off—{Fe(btr)$_2$(NCX)$_2$} shows no SCO, whereas {Fe(btr)$_2$(NCS)$_2$}·H$_2$O shows complete crossover[11]—or it can modify the transition: the network {Fe (bpbd)$_2$(NCS)$_2$}·2Solv

Received: May 3, 2011
Published: October 05, 2011

shows a thermal hysteresis for ethanol and methanol guests, but not for acetone, acetonitrile or 1-propanol.[15]

In contrast to the 2D SCO-CPs mentioned above, no SCO has been observed for the closely related 2D-CPs $\{Fe(4,4'\text{-bipy})_2(NCS)_2\}\cdot n$Solv where 4,4′-bipy is the well-known bis-monodentate building block 4,4′-bipyridine and Solv represents a variety of solvents including nitromethane, nitrobenzene, acetone, methanol, toluene, trichloroethene, carbon disulfide, or diethyl ether ($n = 1-3$).[19] Like for the other members of the $\{Fe(L)_2(NCX)_2\}\cdot n$Solv series, self-assembly of Fe(II), NCS^- and 4,4′-bipy produces similar 2D (4,4) grids which stack in a parallel fashion without interpenetration. At 100 K, the crystal structure of all eight of these solvates contained the iron(II) atoms in a high-spin configuration, and magnetic susceptibility measurements on the nitrobenzene and toluene solvates showed no SCO in the temperature range 300−5 K. The lack of SCO in these solvates can be considered somewhat surprising given the similarity between 4,4′-bipy and the other bis-monodentate ligands mentioned above.

Aware of the influence that subtle structural changes have on the electronic configuration of Fe(II) complexes exhibiting ligand field strengths close to the HS-LS state crossing point, we have pursued the search for new solvates of $\{Fe(4,4'\text{-bipy})_2(NCS)_2\}$. Here we report the synthesis of the chloroform solvate of the system $\{Fe(4,4'\text{-bipy})_2(NCX)_2\}\cdot 4CHCl_3$ with X = S (**1·4CHCl$_3$**) or Se (**2·4CHCl$_3$**). Variable temperature magnetic susceptibility, calorimetric measurements, and X-ray structural determinations confirm the occurrence of cooperative spin crossover behavior for both compounds.

RESULTS

Magnetic and Calorimetric Studies. The magnetic properties of **1·4CHCl$_3$** and **2·4CHCl$_3$** are shown in Figure 1 in the form of $\chi_M T$ vs T plots, where χ_M is the molar magnetic susceptibility and T is the temperature. Given the extreme lability of the $CHCl_3$ molecules, wet single crystals of **1·4CHCl$_3$** were transferred directly from the mother liquor into a sealed Teflon sample holder. The actual sample mass was evaluated from the resulting dry unsolvated compound **1**. The estimated mass in different experiments was typically in the range 130−150 mg. **1·4CHCl$_3$** was quickly cooled down to 50 K (black diamonds in Figure 1a). At this temperature $\chi_M T$ was about 1.62 cm^3 K mol^{-1}, and is practically constant on warming to 123 K (1.75 cm^3 K mol^{-1}). This value of $\chi_M T$ is consistent with the presence of a 50:50 mixture of iron(II) ions in the HS and in the LS state and corresponds to trapping of 50% of the iron(II) ions in the HS state because of slow kinetics (see below). Between 125 and 131 K the $\chi_M T$ value undergoes a sudden rise to 2.21 cm^3 K mol^{-1} followed by a small decrease, which can probably be ascribed to the occurrence of a crystallographic phase transition. The small decrease in $\chi_M T$ would represent relaxation of the system from the thermally trapped phase to the thermodynamically stable phase characterized by a smaller $\chi_M T$ value at higher temperatures. In the temperature interval 156−200 K, $\chi_M T$ is about 3.40 cm^3 K mol^{-1}, indicating that the LS centers have been thermally promoted to the HS state. Then a cooling-warming cycle was performed on the same sample in the temperature range 200−50 K (open circles). Interestingly, **1·4CHCl$_3$** displays a complete two-step cooperative ST characterized by the critical temperatures T_{c1}^{down} = 143.1 K, T_{c2}^{down} = 91.2 K, T_{c1}^{up} = 150.7 K, and T_{c2}^{up} = 112.2 K. The two steps are separated by a plateau ($\chi_M T$ = 1.70 cm^3 K mol^{-1})

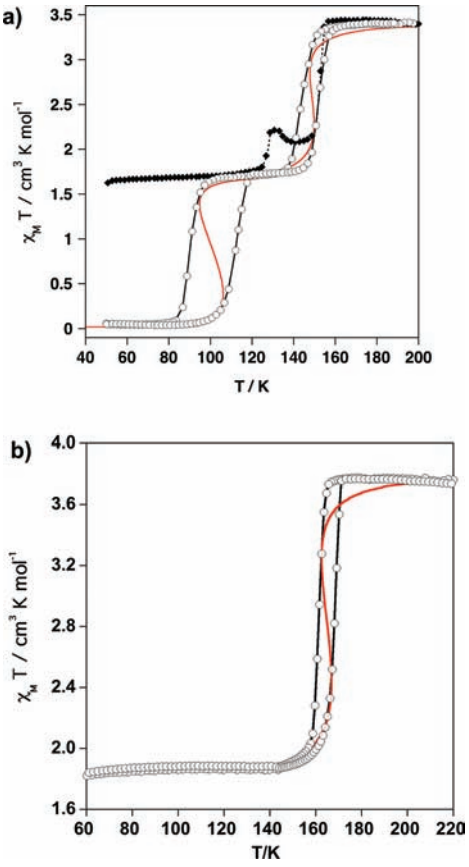

Figure 1. Magnetic behavior of **1·4CHCl$_3$** (a) and **2·4CHCl$_3$** (b). Black solid lines are to guide the eyes, while the red solid line corresponds to the simulation of the spin transition (see text).

that is about 34 and 24 K wide for the cooling and warming modes, respectively. Hysteresis loops of approximately 7.6 and 21 K width characterize the high- and low-temperature STs, respectively. The same results were observed in subsequent cycles. The magnetic behavior of the same sample in the desolvated state corresponds to that of an iron(II) ion in the HS state over the whole range of temperatures (see Supporting Information).

The $CHCl_3$ molecules were less labile in the compound **2·4CHCl$_3$** and, consequently, comparable magnetic behaviors were observed for wet and freshly prepared dry samples (kept at ca. 250 K). $\chi_M T$ is equal to 3.75 cm^3 K mol^{-1} at 200 K indicating that the compound is in the HS state at this temperature. This value remains constant after cooling down to 167 K after which **2·4CHCl$_3$** undergoes a cooperative half ST, $\chi_M T$ dropping to attain a value of 1.87 cm^3 K mol^{-1} at 140 K, and remaining essentially constant down to 50 K (open circles, Figure 1b). Below this temperature $\chi_M T$ slightly decreases, most probably because of zero-field splitting of the remaining HS iron(II) ions. In the warming mode, the $\chi_M T$ values around the SCO region do not match those observed for the cooling mode, creating a hysteresis loop 6.6 K wide, characterized by T_c^{down} = 161.7 K and T_c^{up} = 168.3 K.

Differential scanning calorimetry (DSC) studies were performed in the temperature interval 300−120 K for $CHCl_3$-wet single crystals of **1·4CHCl$_3$** and for dry samples of compound **2·4CHCl$_3$** in sealed aluminum pans. The actual sample mass of

dx.doi.org/10.1021/ic200932w |Inorg. Chem. 2011, 50, 10633–10642

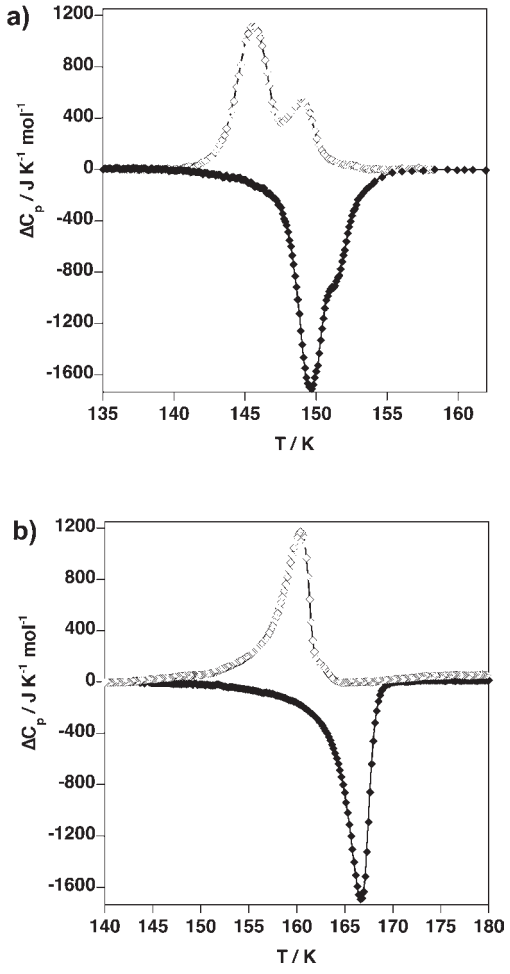

Figure 2. Calorimetric measurements for $\mathbf{1}\cdot\mathbf{4CHCl_3}$ and $\mathbf{2}\cdot\mathbf{4CHCl_3}$ in the cooling (open diamonds) and warming (closed diamonds) modes.

$\mathbf{1}\cdot\mathbf{4CHCl_3}$ was evaluated from the resulting dry unsolvated compound **1**, being typically in the range 25−35 mg. Because the lowest temperature limit of the calorimeter was 120 K the low-temperature step of $\mathbf{1}\cdot\mathbf{4CHCl_3}$ could not be monitored.

Anomalous variation of the molar specific heat, ΔC_p, versus T for the cooling and warming modes is displayed in Figure 2. The critical temperatures deduced from this experiment, T_c^{down} = 145.6 and 160.4 K and T_c^{up} = 149.6 and 166.8 K for $\mathbf{1}\cdot\mathbf{4CHCl_3}$ and $\mathbf{2}\cdot\mathbf{4CHCl_3}$, respectively, agree quite well with those deduced from magnetism for the first step of $\mathbf{1}\cdot\mathbf{4CHCl_3}$ and for $\mathbf{2}\cdot\mathbf{4CHCl_3}$. The shoulders observed for the high-temperature step in $\mathbf{1}\cdot\mathbf{4CHCl_3}$ (cooling and heating modes) may reflect changes in cooperativity related to subtle structural modifications occurring during the spin state change and have also been detected from the derivative of $\chi_M T$ vs T (see Supporting Information, Figure S1). The enthalpy (ΔH) and entropy (ΔS) variations associated with each mode are, respectively, 4.5 kJ mol^{-1} and 31.0 J K^{-1} mol^{-1} (cooling mode) and 5.9 kJ mol^{-1} and 35.4 J K^{-1} mol^{-1} (heating mode) for $\mathbf{1}\cdot\mathbf{4CHCl_3}$ and 5.8 kJ mol^{-1} and 36.1 J K^{-1} mol^{-1} (cooling mode) and 6.7 kJ mol^{-1} and 40.2 J K^{-1} mol^{-1} (warming mode) for $\mathbf{2}\cdot\mathbf{4CHCl_3}$.

The enthalpy, ΔH, and entropy, ΔS, parameters associated with the two-step ST observed for $\mathbf{1}\cdot\mathbf{4CHCl_3}$ and $\mathbf{2}\cdot\mathbf{4CHCl_3}$ have also been estimated by applying the regular solutions model assuming each step is like two independent events:[20]

$$\ln[(1-\gamma_{HSi})/(\gamma_{HSi}-f_{HSi})] = \Delta H_i + \Gamma_i(1+f_{HSi}-2\gamma_{HSi})/RT - \Delta S/R \qquad (i=1,2) \tag{1}$$

where $f_{HSi} = (\chi_M T)_{LTi}/[(\chi_M T)_{HSi} - (\chi_M T)_{LSi}]$ is the residual HS molar fraction, $(\chi_M T)_{LTi}$ is the $\chi_M T$ value at low temperature [105 K ≤ T ≤ 135 K for the ST i = 1 occurring in the interval 160−105 and 40 K ≤ T ≤ 90 K for the ST i = 2 occurring in the interval 130−50 K], γ_{HS} is the HS molar fraction expressed as follows:

$$\gamma_{HSi} = [(\chi_M T)_{mi} - (\chi_M T)_{LSi}]/[(\chi_M T)_{HSi} - (\chi_M T)_{LSi}] \tag{2}$$

$(\chi_M T)_{mi}$ is the experimental $\chi_M T$ value, and $(\chi_M T)_{LSi}$ and $(\chi_M T)_{HSi}$ correspond to the expected values for the fully populated LS and HS states. Given that the plateau between the two transitions is practically at 50% of conversion and that the transition is complete, it is sensible to consider f_{HSi} = 0 (i = 1, 2). Simulation of the experimental data was then performed with $(\chi_M T)_{HSi}$ = 3.40 and 1.70 cm^3 K mol^{-1} and $(\chi_M T)_{LSi}$= 1.70 and 0 cm^3 K mol^{-1} for i = 1 and 2, respectively. The best simulation of the experimental data for $\mathbf{1}\cdot\mathbf{4CHCl_3}$ gives ΔH_1 = 5.18 kJ mol^{-1}, ΔS_1 = 35 J K^{-1} mol^{-1}, and Γ_1 = 2.8 kJ mol^{-1} for the high-temperature transition and ΔH_2 = 3.55 kJ mol^{-1}, ΔS_2 = 35 J K^{-1} mol^{-1}, and Γ_2 = 2.6 kJ mol^{-1} for the low-temperature transition (see the red line in Figure 1a). The best simulation of the experimental data for $\mathbf{2}\cdot\mathbf{4CHCl_3}$ gives ΔH_1 = 6.5 kJ mol^{-1}, ΔS_1 = 40.0 J K^{-1} mol^{-1}, and Γ_1 = 3.3 kJ mol^{-1}. It is worth noting that the experimental average values $\Delta H_1^{av,exp}$ = 5.2 kJ mol^{-1} and $\Delta S_1^{av,exp}$ = 33.2 J K^{-1} mol^{-1} for $\mathbf{1}\cdot\mathbf{4CHCl_3}$ and $\Delta H_1^{av,exp}$ = 6.2 kJ mol^{-1} and $\Delta S_1^{av,exp}$ = 38.1 J K^{-1} mol^{-1} for $\mathbf{2}\cdot\mathbf{4CHCl_3}$ agree satisfactorily with those obtained from simulation with eq 1. Differences between simulated and experimental curves are within the level of error expected for the applied model.

These thermodynamic parameters appear reasonable when compared with those previously reported for other iron(II) spin crossover compounds.[21] For example, the closely related 2D SCO polymer $[Fe(btr)_2(NCS)_2]\cdot H_2O$ displays a complete cooperative ST, with critical temperatures T_c^{down} = 121 K and T_c^{up} = 145 K, with ΔH = 10.0 kJ mol^{-1}, ΔS = 76 J K^{-1} mol^{-1}, and Γ = 4.7 kJ mol^{-1}.[22] Note that the thermodynamic parameters estimated for $\mathbf{1}\cdot\mathbf{4CHCl_3}$ correspond to half-ST and should be multiplied by 2 to get comparable values.

Crystal Structures. Crystals of $\mathbf{1}\cdot\mathbf{4CHCl_3}$ were exceedingly prone to solvent loss. Selected crystals picked up from the mother liquor were soaked in inert oil (NParatone) and mounted immediately on a goniometer at 120 K, in the center of the plateau where equal numbers of HS and LS species are present (according to the magnetic data). This allowed the crystal structure to be recorded at this temperature, but despite many attempts, we could not solve the crystal structure in the HS state because of the crystals deteriorating in less than 1 h at 190 K. However, we were able to obtain the cell parameters, which indicate a change of space group from monoclinic $C2/c$ at 120 K to monoclinic $P2/c$ at 190 K (a = 11.607(2) Å, b = 11. 560(2) Å, c = 16.057(4) Å, β = 103.73(2)°). The fully LS state was not reached because our cryostat cannot reach temperatures below 90 K. The crystal structure of $\mathbf{2}\cdot\mathbf{4CHCl_3}$ was solved at both

Table 1. Crystal Data for $1\cdot4CHCl_3$, and $2\cdot4CHCl_3$

	$1\cdot4CHCl_3$	$2\cdot4CHCl_3$	
	120 K	100 K	200 K
empirical formula	$C_{52}H_{40}N_{12}S_4Cl_{24}Fe_2$	$C_{52}H_{40}N_{12}Se_4Cl_{24}Fe_2$	$C_{26}H_{20}N_6Se_2Cl_{12}Fe$
Mr	1923.70	2111.30	1055.66
crystal system	monoclinic	monoclinic	monoclinic
space group	*C*2/*c*	*C*2/*c*	*P*2/*c*
a (Å)	22.6810(8)	22.693(2)	11.499(5)
b (Å)	22.6170(6)	22.608(2)	11.505(4)
c (Å)	17.2920(7)	17.291(2)	17.854(5)
β (deg)	117.757(5)	116.933(2)	117.94(2)
V (Å^3)	7849.7(5)	7908.9(12)	2086.7(13)
Z	4	4	2
D_c (mg cm^{-3})	1.628	1.773	1.680
F(000)	3840	4128	1032
μ (Mo−K$_\alpha$) (mm^{-1})	1.337	3.062	2.902
crystal size (mm)	0.10 × 0.04 × 0.04	0.10 × 0.10 × 0.05	0.10 × 0.10 × 0.05
total reflections	9281	6853	2164
no. of reflections [$I > 2\sigma(I)$]	4667	5613	1908
R_1 [$I > 2\sigma(I)$][a]	0.0558	0.0444	0.0530
wR [$I > 2\sigma(I)$][a]	0.1023	0.0980	0.1353
S	0.918	1.050	1.048

[a] $R_1 = \Sigma||F_o| - |F_c||/\Sigma|F_o|$; $wR = [\Sigma w(F_o^2 - F_c^2)^2/\Sigma w(F_o^2)^2]^{1/2}$. $w = 1/[s^2(F_o^2) + (mP)^2 + nP]$ where $P = (F_o^2 + 2F_c^2)/3$; m = 0.0620 (**1**), 0.0594 (**2**, 100 K), and 0.0950 (**2**, 200 K); n = 0.0000 (**1**), 16.6439 (**2**, 100 K), and 4.3759 (**2**, 200 K).

100 and 200 K. Table 1 contains crystallographic data for both compounds.

At low temperatures, the structures of both $\mathbf{1\cdot4CHCl_3}$ and $\mathbf{2\cdot4CHCl_3}$ are in the monoclinic *C*2/*c* space group with similar crystal parameters indicating they are strictly isostructural, at least in the intermediate mixed spin-state phase. In this phase, [120 K ($\mathbf{1\cdot4CHCl_3}$) and 100 K ($\mathbf{2\cdot4CHCl_3}$)], there are two crystallographically distinct iron(II) sites, Fe1 and Fe2, lying on a 2-fold axis running along the [010] direction, creating pseudo-octahedral [FeN_6] centers. Figure 3 depicts both coordination sites individually, together with the corresponding atom numbering within the asymmetric unit. Table 2 contains representative bond angles and distances. The four equatorial positions are occupied by the 4,4′-bipyridine ligands, while the axial positions are occupied by the thiocyanate anions. The Fe−N_{eq} bond lengths, in the range 1.982−2.003 Å for Fe1 and 2.208−2.258 Å for Fe2, are slightly larger than the Fe−N_{ax} bond lengths: 1.938(4) Å ($\mathbf{1\cdot4CHCl_3}$) and 1.938(5) Å ($\mathbf{2\cdot4CHCl_3}$) for Fe1 and 2.094(4) Å ($\mathbf{1\cdot4CHCl_3}$) and 2.104(5) Å ($\mathbf{2\cdot4CHCl_3}$) for Fe2. The bond lengths found for the Fe1 and Fe2 sites for both compounds are typical of iron(II) in the LS and HS states, respectively, in agreement with the magnetic data. Consistent with this observation, the N−Fe1−N bond angles differ insignificantly from those expected for a regular octahedron, but the differences are more marked for N−Fe2−N. The NCS^- and $NCSe^-$ groups are practically linear and are tilted by 6.6° ($\mathbf{1\cdot4CHCl_3}$) [7.2° ($\mathbf{2\cdot4CHCl_3}$)] and 15.3° ($\mathbf{1\cdot4CHCl_3}$) [12.1° ($\mathbf{2\cdot4CHCl_3}$)] for Fe1 and Fe2, respectively, with respect to the (SC)N−Fe−N(CS) axis.

The 4,4′-bipyridine ligands bridge the iron sites, defining an almost square grid (Figure 4). The average Fe···Fe distance through the 4,4′-bipyridine is 11.3 Å ($\mathbf{1\cdot4CHCl_3}$) [11.4 Å ($\mathbf{2\cdot4CHCl_3}$)], while the shortest Fe···Fe separation between adjacent layers is 9.637(2) Å ($\mathbf{1\cdot4CHCl_3}$) [9.616(2) Å ($\mathbf{2\cdot4CHCl_3}$)] and 9.630(2) Å ($\mathbf{1\cdot4CHCl_3}$) [9.606(2) Å ($\mathbf{2\cdot4CHCl_3}$)], which correspond to Fe1···Fe1 and Fe2···Fe2 distances, respectively. The separation between two consecutive layers (Figures 5 and 6), measured from the average plane defined by the iron atoms, is 7.651 Å ($\mathbf{1\cdot4CHCl_3}$) and 7.708 Å ($\mathbf{2\cdot4CHCl_3}$). The pyridine rings of the 4,4′-bipyridine ligands are not coplanar, the angle between the pyridine rings containing the atoms N1 and N5, N2 and N6, and N3 and N7 being 53.48°, 59.14°, and 38.49° for $\mathbf{1\cdot4CHCl_3}$ and 55.82°, 59.14°, and 38.49° Å for $\mathbf{2\cdot4CHCl_3}$, respectively. The pyridine moieties coordinated to Fe1 are tilted in a propeller fashion defining angles in the range 35−42° with respect to the two perpendicular planes defined by N(3)−N(4)−N(2)−N(4) and N(1)−N(4)−N(1)−N(4). These angles are more irregularly distributed around the Fe2 site; the pyridine ring containing the atom N7 defines an angle of 2.98° ($\mathbf{1\cdot4CHCl_3}$) [6.74° ($\mathbf{2\cdot4CHCl_3}$)], while the opposite pyridine N6 forms an angle of 78.94° ($\mathbf{1\cdot4CHCl_3}$) [72.64° ($\mathbf{2\cdot4CHCl_3}$)] and the "N5" pyridines deviates 20.17° ($\mathbf{1\cdot4CHCl_3}$) [10.32° ($\mathbf{2\cdot4CHCl_3}$)].

In this intermediate mixed spin-state phase, both derivatives display a large number of significant intermolecular contacts (smaller than the sum of the van der Waals distances) involving guest···guest and host···guest moieties (Table 3). It should be noted that despite the isostructural nature of both compounds the number and distribution of these contacts is not exactly the same.

At 200 K the crystals of $\mathbf{2\cdot4CHCl_3}$ are in the monoclinic space group *P*2/*c*. At this temperature there is only one unique iron(II) site, lying on the 2-fold axis running parallel to *b*, which also contains the N3−Fe−N2 bonds (see Figure 7 and Table 2). The Fe−N_{eq} bond distances are in the range 2.182(10)-2.250(10) Å and the Fe−N_{ax} distances are 2.133(8) Å, which is consistent

dx.doi.org/10.1021/ic200932w |*Inorg. Chem.* 2011, 50, 10633–10642

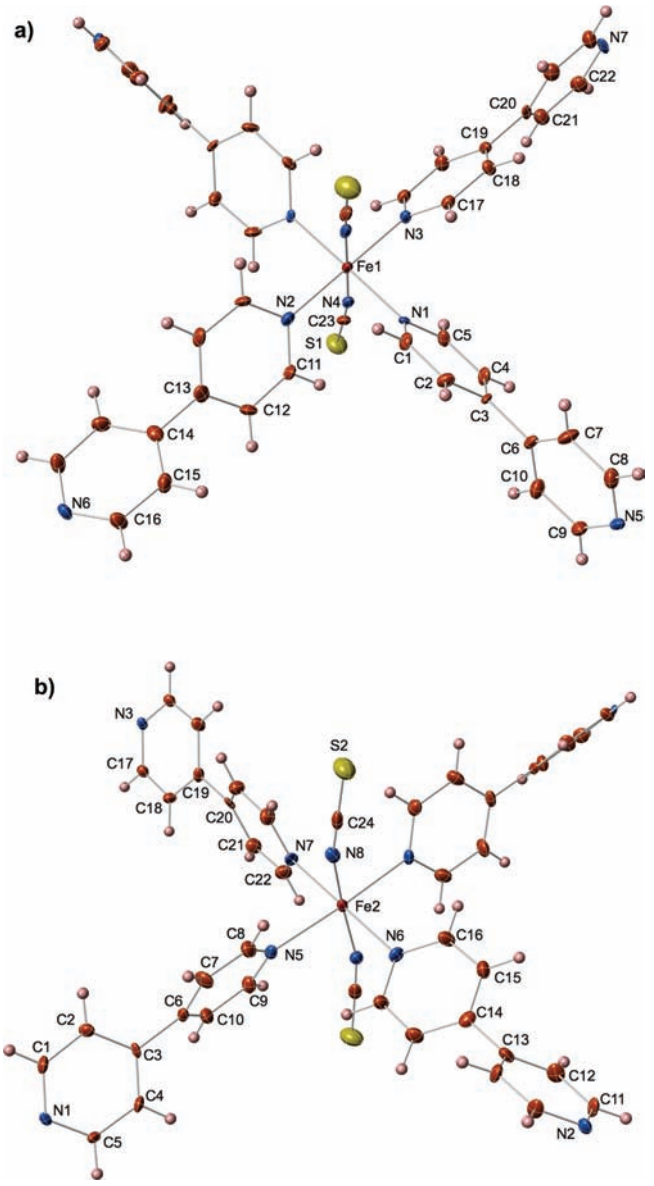

Figure 3. Fragment of the structure of **1·4CHCl$_3$** (120 K) showing the atom numbering of asymmetric units of sites Fe1 (a) and Fe(2) (b). Same atom numbering applies for **2·4CHCl$_3$** (100 K) since both compounds are isostructural.

with the iron(II) ion being in the HS state. The $NCSe^-$ group is practically linear and is tilted 11.6° with respect to the N4—Fe—N4 axis.

The average Fe1····Fe1 distance through 4,4′-bipyridine is 11.502(2) Å while the shortest Fe1····Fe1 separation between adjacent layers is 9.630(2) Å. The separation between two consecutive layers, measured from the average plane defined by the iron atoms, is 7.886 Å. The angle defined by the two pyridine rings of each 4,4′-bipy ligand is 50.72° for the 4,4′-bipy containing the N(1) atom and 41.42° for the 4,4′-bipy containing the N(2) and N(3) atoms. The pyridine moieties coordinated to Fe1 are tilted in a propeller fashion, defining angles in the range 7.99—49.41° with respect to the planes defined by the atoms N(2)—N(4)—N(3)—N(4) and N(1)—N(4)—N(1)—N(4). The orientation of the pyridine rings is one of the most noticeable differences between the high-and low-spin structures. At both high and low temperatures, the HS iron atoms have one of their four coordinated pyridine ligands almost perfectly eclipsed with the SCN—Fe—NCS axis, whereas the LS centers have all four pyridine ligands canted so that a staggered arrangement is achieved. This implies a significant rotation of one of the pyridine rings upon changing spin state. In this HS phase the number of significant intermolecular contacts is less than 50% of those observed in the intermediate mixed spin-state phase (Table 3).

Table 2. Selected Bond Lengths [Å] and Angles [deg] for 1·4CHCl$_3$, and 2·4CHCl$_3$

	1·4CHCl$_3$	2·4CHCl$_3$	
	120 K	100 K	200 K
Fe(1)—N(1)	2.000(3)	2.003(4)	2.225(6)
Fe(1)—N(2)	1.988(5)	1.986(7)	2.182(10)
Fe(1)—N(3)	1.998(5)	1.982(7)	2.250(10)
Fe(1)—N(4)	1.952(4)	1.938(5)	2.133(8)
Fe(2)—N(5)	2.258(3)	2.247(5)	
Fe(2)—N(6)	2.243(5)	2.233(7)	
Fe(2)—N(7)	2.218(5)	2.208(7)	
Fe(2)—N(8)	2.094(4)	2.104(5)	
N(1)—Fe(1)—N(2)	89.71(9)	90.0(2)	90.1(2)
N(1)—Fe(1)—N(3)	90.29(9)	90.0(2)	89.9(2)
N(1)—Fe(1)—N(4)	90.14(13)	90.6(2)	91.0(3)
N(2)—Fe(1)—N(3)	180.000(1)	180.000(1)	180.000(2)
N(2)—Fe(1)—N(4)	89.70(10)	90.0(2)	88.1(2)
N(3)—Fe(1)—N(4)	90.30(10)	90.0(2)	91.9(2)
N(5)—Fe(2)—N(6)	91.84(9)	91.8(2)	
N(5)—Fe(2)—N(7)	88.16(9)	88.2(2)	
N(5)—Fe(2)—N(8)	90.11(13)	90.5(2)	
N(6)—Fe(2)—N(7)	180.000(1)	179.997(1)	
N(6)—Fe(2)—N(8)	87.00(10)	87.7(2)	
N(7)—Fe(2)—N(8)	93.00(10)	92.3(2)	

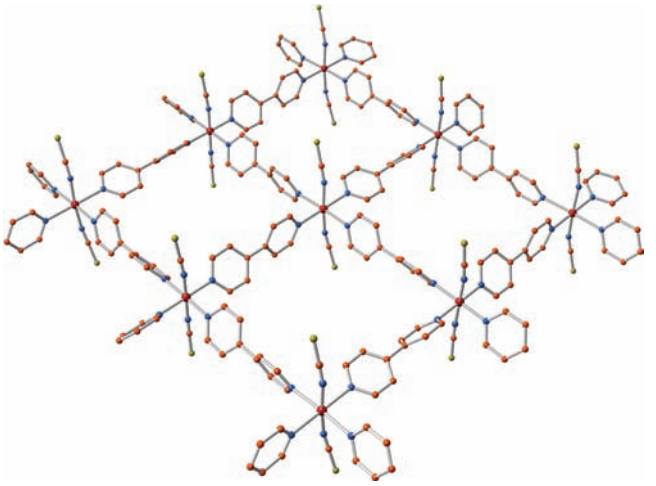

Figure 4. Fragment of a layer of **1·4CHCl$_3$**.

DISCUSSION

The 4,4′-bipy building block has been used as an ancillary bridging ligand for the synthesis of a number of iron(II) SCO

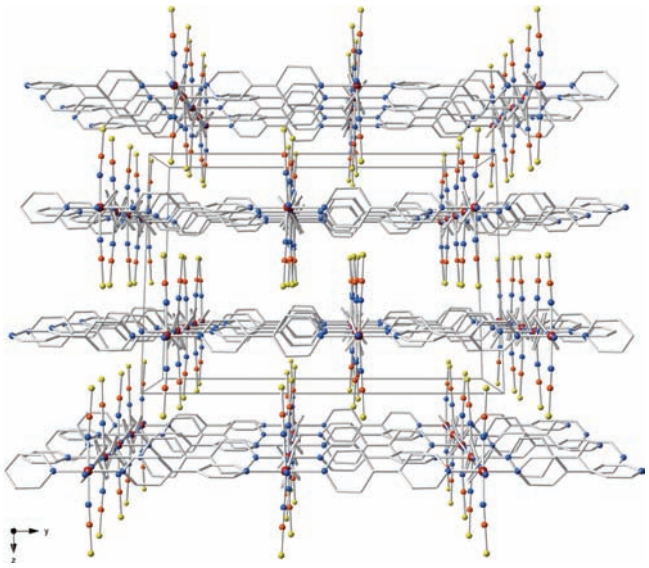

Figure 5. Perspective view of the crystal packing view along [100] for **1·4CHCl$_3$**. Solvent molecules have been removed for clarity.

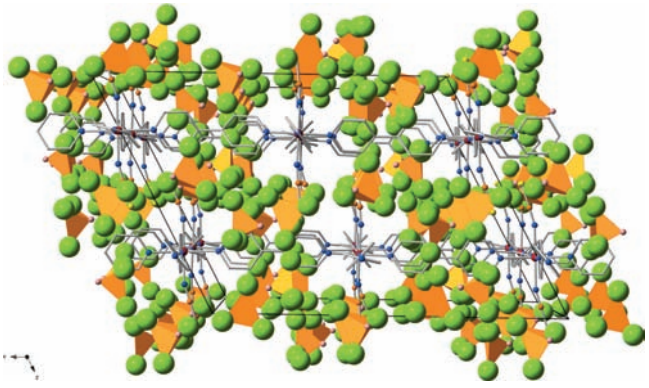

Figure 6. Perspective view of the crystal packing along [100] including the $CHCl_3$ molecules for **1·4CHCl$_3$**.

compounds ranging from discrete binuclear[23,24] species to 1D[25−28] and 3D[29] coordination polymers. In contrast, when 4,4′-bipy in combination with NCS^- are the only coordinating species, the resulting 2D CP [Fe(4,4′-bipy)$_2$(NCS)$_2$] (**1**)[30] show magnetic properties characteristic of the HS state suggesting that the 4,4′-bipy ligand induces relatively weak ligand field. On the basis of the crystal structure of the isostructural Ni derivative,[31] strong intermolecular interactions between the pyridine rings belonging to consecutive layers take place in both unsolvated compounds (C···C in the range 3.45−3.70 Å). This could be the cause of the large distortion observed in the coordination octahedron, Σ = 39.4°, and hence of the stabilization of the HS state in the Fe(II) derivative. The parameter Σ is the sum of the deviation from 90° of the 12 N−Fe−N angles of the [FeN_6] core [$\Sigma(|\varphi - 90|)$],[32a] a simplified form of the so-called bond angle variance parameter (σ^2).[32b]

Inclusion of solvents in **1** to afford **1·*n*S** [*n*S = 2(trichloroethene), 2(toluene), 2(nitrobenzene), 2(diethylether), 4(acetone), 3(methanol)] does not affect the essential structure of the 2D network. However, remarkable differences in the interlayer spacing and in the relative angles defined between the pyridine rings were observed for these solvates (Table 4).[19] In addition, a concomitant substantial drop of the Σ parameter to values in the range 7−21° takes place for the **1·*n*S** solvates (Table 4). Nevertheless, this reduction of Σ is not enough to destabilize the HS state. This behavior strongly contrasts with the cooperative ST properties observed for the chloroform solvate **1·4CHCl$_3$** and its isostructural selenocyanate homologue **2·4CHCl$_3$**. For the latter compounds, the interlayer spacing necessary to accommodate the four molecules of $CHCl_3$, about 7.7 Å, is about 9% larger than in **1·4acetone**,[19] and about 70% larger than that of the unsolvated [Fe(4,4′-bipy)$_2$(NCS)$_2$] (4.458 Å) deduced from its isostructural Ni compound.[32]

On the basis of the average Fe−N bond distance, $\langle d_{Fe-N} \rangle$, and Σ parameters displayed in Table 4, it is difficult to find evidence that might help us to understand the marked difference between the magnetic behaviors of **1·*n*S** and the title compounds. The average $\langle d_{Fe-N} \rangle$ = 2.191 ± 0.012 Å found for the **1·*n*S** series is essentially identical to that found for the HS Fe sites in the $CHCl_3$ solvates. Although Σ varies rather widely (7.20°−20.84°) in the **1·*n*S** series, these values are comparable to those found at the middle of the plateau for Fe(2) in **1·4CHCl$_3$** and **2·4CHCl$_3$** and that found for the HS iron(II) site at 200 K for **2·4CHCl$_3$**. Interestingly, when **2·4CHCl$_3$** moves from the HS phase (Fe, Σ_{HS} = 10.0°, T = 200 K) to the intermediate mixed spin-state phase, where the Fe(II) ions are regularly distributed in LS and HS sites, the Σ value splits accordingly into two distinct values showing a decrease and an increase of about 7−8° for the LS site (Fe1, Σ_{LS} = 3.8°, T = 100 K) and HS site (Fe2, Σ_{HS} = 17.9°, T = 100 K), respectively. The additional increase of about 55% observed for Σ_{HS} could be the cause of the stabilization of the Fe2 HS site and observation of the intermediate phase. This should also be applicable for the **1·4CHCl$_3$** derivative.

It is worth noting the significantly larger deviation from 180° found for the Fe−N−CX angle in **1·*n*S** (except for the acetone solvate) with respect to the title compounds (Table 4). It is well-known that this angle is sensitive to the spin state of Fe(II) and tends to be closer to 180° in the LS state. Indeed, this angle is about 8.7° and 4.4° larger for the LS site than for the HS site in **1·4CHCl$_3$** and **2·4CHCl$_3$**, respectively. Hence, it is sensible to consider that this larger deviation from 180° involves some additional stabilization of the HS state in **1·*n*S**.

The occurrence or absence of SCO behavior has been recently discussed in similar terms for other 2D SCO-CPs.[1j,33,34] For example, the complex [Fe(btre)$_2$(NCS)$_2$] (btre = 1,2-bis(1,2,4-triazol-4yl)ethane), closely related to the well-known [Fe(btr)$_2$(NCS)$_2$] complex, is paramagnetic even at pressures as high as 12 kbar showing marked destabilization of the LS state. A comparative analysis of the Fe coordination centers of these compounds showed that the btre derivative has Σ and $\langle d_{Fe-N} \rangle$ values [21.2° and 2.186(3) Å] larger than those observed for the btr derivative [14.8° and 2.164(3) Å]. Furthermore, the interlayer spacing for the btre derivative is the same as that of the btr derivative in the LS state, which facilitates the occurrence of strong π−π and S···S interactions between consecutive layers in the former and probably enhances stabilization of the HS state.[33] Similarly, complete desolvatation of the doubly interpenetrated 2D SCO porous compound [Fe(bped)$_2$(NCS)$_2$]·3EtOH bped = (dl-1,2-bis(4′-pyridyl)-1,2-ethanediol) induces significant structural changes at the Fe center and stabilization of the LS state. These changes include for the HS state decrease of Σ and $\langle d_{Fe-N} \rangle$ from 15.6° to 2.0°, and from 2.183 Å to 2.147 Å, respectively, as well as marked straightening of the Fe−NCS angle from 168.5° to 180°.[34]

Table 3. Host···Guest and Guest···Guest Short Intermolecular Contacts (Å)

1·4CHCl$_3$ (T = 120 K)[a]

S(1)··C(25)^{i} = 3.571(5)	C(15)··Cl(6)^{v} = 3.630(4)	Cl(7)··C(6)^{viii} = 3.561(5)	Cl(8)··C(19)^{ix} = 3.502(2)
S(2)··C(28)^{ii} = 3.542(6)	C(23)··Cl(6) = 3.590(5)	Cl(7)··C(7)$^{vii\ i}$ = 3.615(5)	Cl(8)··C(20)^{ix} = 3.636(2)
S(2)··Cl(3)^{iii} = 3.518(2)	Cl(3)··C(9)^{ii} = 3.584(5)	Cl(7)··C(8)^{viii} = 3.603(5)	Cl(9)··C(4)^{x} = 3.450(5)
S(1)··Cl(6) = 3.533(4)	Cl(3)··C(18)^{vi} = 3.592(4)	Cl(7)··C(9)^{viii} = 3.407(5)	Cl(9)··C(4)^{x} = 3.450(5)
C(14)·C(16)^{iv} = 3.604(5)	Cl(3)·C(24)^{vii} = 3.605(5)	Cl(7)··C(10)^{viii}= 3.434(5)	Cl(10)··C(2)^{viii}= 3.609(5)
C(3)··Cl(5) = 3.562	Cl(5)··Cl(1)^{ii} = 3.566(2)	Cl(8)··C(18)^{ix} = 3.391(4)	Cl(10)··C(12)^{viii}= 3.599(6)
C(4)··Cl(5) = 3.579(5)	Cl(5)··Cl(8) = 3.596(2)	Cl(8)··C(19)^{ix} = 3.502(2)	C(14)··Cl(11) = 3.516(3)

2·4CHCl$_3$ (T = 100 K)[b]

Se(1)··C(25)^{i} = 3.666(3)	Se(2)··C(28)^{ii} = 3.649(3)	Cl(7)··C(6)^{vii} = 3.533(3)	Cl(9)··C(4)^{ix} = 3.399(3)
Se(2)··C(28)^{ii} = 3.649(3)	Cl(3)··C(9)^{ii} = 3.606(2)	Cl(7)··C(7)^{vii} = 3.614(3)	Cl(10)··C(12)^{vii} = 3.642(3)
C(24)··Cl(3)^{iii} = 3.631(2)	Cl(4)··C(15)^{v} = 3.580(3)	Cl(7)··C(8)^{vii} = 3.639(3)	Cl(4)··Cl(11)^{ii} = 3.360(2)
Se(1)··Cl(6) = 3.590(2)	Cl(4)··C(16)^{v} = 3.502(3)	Cl(7)··C(9)^{vii} = 3.414(2)	Cl(5)··Cl(1)^{ii} = 3.541(2)
Se(1)·Cl(10)^{iii} = 3.368(3)	Cl(5)··C(3)= 3.643(3)	Cl(7)··C(10)^{vii}= 3.405(3)	Cl(12)··Cl(9)^{x}= 3.402(3)
Se(2)··Cl(3)^{iv}= 3.686(2)	Cl(6)·C(15)^{vi} = 3.653(3)	Cl(8)·C(18)^{viii} = 3.447(2)	
Se(2)·C(21)^{iii} = 3.542(2)	Cl(6)··C(23) = 3.649(2)	Cl(8)··C(19) = 3.554(3)	

2·4CHCl$_3$ (T = 200 K)[c]

Cl(1)··C(1)^{i} = 3.639(2)	Cl(2)··C(4)^{ii} = 3.355(2)	Cl(4)··C(12)^{iv}= 3.620(2)	Cl(2′)··Cl(5)^{vii}= 3.152(2)
Cl(1)··C(2)^{i} = 3.509(2)	Cl(2)··C(5)^{ii} = 3.482(2)	Cl(1′)··Se^{v} = 3.411(2)	Cl(3′)··C(2)^{ii} = 3.661(2)
Cl(2)··C(3)^{ii} = 3.494(2)	Cl(3)··C(12)^{iii}= 3.542(2)	Cl(2′)··Cl(5)^{vi}= 3.740(2)	Se(1)··C(26)^{iv}= 3.741(2)

[a] (i = $-x$+1, y, $-z$+1/2); (ii = $-x$+3/2, $-y$+1/2, $-z$+1); (iii = x+1/2, $-y$+1/2, z+1/2); (iv = x, $-y$, z−1/2); (v = $-x$+1, $-y$, $-z$+1); (vi = x, y, z−1); (vii = x−1/2, $-y$+1/2,z−1/2); (viii = $-x$+3/2, y+1/2, $-z$+3/2); (ix = $-x$+1, y, $-z$+3/2); (x = $-x$+3/2, $-y$+1/2, $-z$+2). [b] (i = $-x$+1, y, $-z$ +1/2) ; (ii = $-x$ +3/2, $-y$ +1/2, $-z$+1); (iii = x− 1/2, $-y$ +1/2, z− 1/2); (iv = x +1/2, $-y$ +1/2, z +1/2); (v = x, $-y$, z +1/2); (vi = $-x$+1, $-y$, $-z$+1); (vii = $-x$ +3/2, y +1/2, $-z$ +3/2); (viii = $-x$+1, y, $-z$ +3/2); (ix = $-x$ +3/2, $-y$ +1/2, $-z$+2); (x = x, $-y$+1, z− 1/2). [c] (i = x, $-y$−1, z+1/2); (ii = $-x$, y, $-z$−1/2); (iii = $-x$, y−1, $-z$−1/2); (iv = $-x$+1, $-y$, $-z$); (v = x−1, $-y$−1, z−1/2); (vi = x, y−1, z); (vii =$-x$, $-y$−1, $-z$); (viii = $-x$, y, $-z$−1/2).

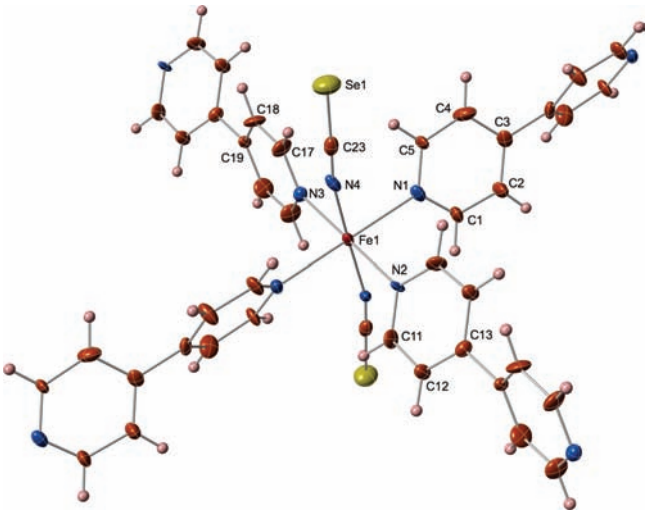

Figure 7. Fragment of the structure of **2·4CHCl$_3$** (200 K) showing the atom numbering of the asymmetric unit.

Compound **1·4CHCl$_3$** experiences a cooperative ST with two well-separated steps, while **2·4CHCl$_3$** undergoes just a half ST. The crystallographic analysis shows that, for both compounds, the high-temperature step occurs concurrently with to a crystallographic phase transition from the $C2/c$ space group in the HS phase to the $P2/c$ space group in the intermediate phase where the HS and LS sites coexist at 50% in an ordered checkerboard-like arrangement. Presumably, the low-temperature step observed for **1·4CHCl$_3$** involves a re-entrant crystallographic phase transition from the intermediate HS-LS ($P2/c$) phase to the LS ($C2/c$) phase. Similar behavior has been recently reported for the 2D coordination polymer {Fe(3-Chloropyridine)$_2$[Pd(CN)$_4$]}.[35] This compound undergoes a strong cooperative two-step SCO characterized by 5−7 K wide hysteresis loops. The first step induces a change from the orthorhombic ($Pnc2$) HS phase, containing one Fe(II) site, to the orthorhombic ($Pmna$) phase where the HS and LS sites are regularly distributed. The second step induces recovery of the of the $Pmna$ space group characterized by one Fe(II) LS site. A second relevant example is the doubly interpenetrated 2D porous SCO system [Fe(bpe)$_2$(NCS)$_2$]·3(acetone), (bpe is 1,2-bis(4′-pyridyl)ethane).[36] The HS phase is characterized by two Fe(II) sites with distinct Σ and $\langle d_{Fe-N}\rangle$ values. In the first step only the site with a more regular coordination environment (Fe2) changes to the LS state, generating a HS(Fe1)-LS(Fe2) checkerboad-like arrangement. This occurs without crystallographic phase transition. However, during the second step when the Fe1 site changes to the LS state the structure changes from the orthorhombic $P2_12_12$ to the tetragonal $P\bar{4}2_1c$ space group. Interestingly, during the first step, the spin-state change in site Fe2 induces a more regular coordination environment in the Fe1 HS site contrary to that observed for the title compound **2·4CHCl$_3$**.

As expected, the average $\langle T_c\rangle$ value for the high-temperature step is larger for **2·4CHCl$_3$** than for **1·4CHCl$_3$**, since it is an experimental fact that $NCSe^-$ induces a stronger ligand field than NCS^-.[1f] However, the difference $\langle T_c\rangle^{Se} - \langle T_c\rangle^{S}$ = 16.7 K is much smaller than observed for the series of mononuclear compounds [Fe(L)$_2$(NCX)$_2$], where L is an α-diimine ligand, where $\langle T_c\rangle^{Se} - \langle T_c\rangle^{S}$ is typically in the range 50−100 K.[11] For the

dx.doi.org/10.1021/ic200932w |Inorg. Chem. 2011, 50, 10633–10642

Table 4. Average Fe−NCS, Fe−N(py), and Fe−N_6 Bond Lengths (Å), Tilt Angle of the Fe−NCS (deg) Moiety, Angular Distortion of the Fe−N_6 Bonds (deg) with Respect to the Regular Octahedron, and Interlayer Spacing Calculated from the Average Plane Defined by the Fe(II) Atoms (Å) for $[Fe(4,4'\text{-bipy})_2(NCS)_2]\cdot nS_i$ [a] and $1\cdot 4CHCl_3$ and $2\cdot 4CHCl_3$

	Compound[b]					
	1·2S1	**1·2S2**	**1·2S3**	**1·2S4**	**1·4S5**	**1·3S6**
T/K	100	100	100	100	100	100
Fe−NCS	2.115(2)	2.106(4)	2.113(2)	2.114(2)	2.133(12)	2.125(2)
$\langle d_{FeN(py)} \rangle$	2.223(2)	2.233(5)	2.248(2)	2.211(3)	2.227(2)	2.229(2)
$\langle d_{FeN6} \rangle$	2.187(2)	2.190(5)	2.203(2)	2.178(3)	2.196(2)	2.194(2)
Fe−N−CS	147.22(14)	157.6(4)	153.21(13)	146.9(2)	166.9(9)	156.8(2)
Σ	17.1	11.9	15.1	9.5	7.2	20.8
$\langle d_{Fe\cdots Fe} \rangle$	5.874	5.590	6.190	6.279	7.037	5.423

	Compound				
	1·4CHCl₃			**2·4CHCl₃**	
T/K	120		200	100	
site	Fe1	Fe2	Fe	Fe1	Fe2
Fe−NCX	1.952(4)	2.094(4)	2.133(8)	1.938(5)	2.104(5)
$\langle d_{FeN(py)} \rangle$	1.996(5)	2.244(5)	2.221(10)	1.993(7)	2.234(7)
$\langle d_{FeN6} \rangle$	1.982(5)	2.194(5)	2.191(9)	1.975(7)	2.190(5)
Fe−N−CS	173.4(3)	164.7(3)	168.4(7)	172.8(5)	167.9(5)
Σ	2.9	19.7	10.0	3.8	17.9
$\langle d_{Fe\cdots Fe} \rangle$	7.651		7.886	7.708	

[a] S1: trichloroethene; S2: 2toluene; S3: nitrobenzene; S4: diethylether; S5: acetone; S6: methanol. [b] Taken from ref 19.

related 2D coordination polymer $[Fe(btr)_2(NCX)_2]\cdot nS$ this difference, 80 K ($\langle T_c \rangle^S$ = 134 K[11] and $\langle T_c \rangle^{Se}$ = 214 K[12]), is also considerably larger than that found in the present work.

The lack of low-temperature ST for **2·4CHCl₃** is an unexpected result. In principle, one should expect a second step about 16.7 K higher than that found for **1·4CHCl₃**. Indeed, the Fe(2) sites are virtually identical for both compounds. However, despite their isostructural character, the number and distribution of the short intermolecular contacts found for both derivatives are different. Subtle packing effects may not only block the second step in **2·4CHCl₃** but also be at the origin of the small separation between the observed $\langle T_c \rangle^{Se} - \langle T_c \rangle^{S}$ value in the present case. Half SCO behavior involving crystallographic phase transition has been reported for a small number of coordination polymers. For example, the 2D coordination polymer $\{Fe(3\text{-Fluoropyridine})_2[(Au(CN)_2]_2\}$ undergoes simultaneously a cooperative half ST and crystallographic transition from the monoclinic space group ($P2_1/c$) (HS phase) to the triclinic ($P\bar{1}$) space group (HS-LS phase) at about 140 K. It is worth noting that this compound displays complete two-step SCO at pressures higher than 0.18 GPa.[37] The 3D SCO system $\{Fe(5\text{-Bromopyrimidine})_2[(Au(CN)_2]_2\}$ shows a strongly cooperative half SCO centered at 158 K characterized by a hysteresis 18 K wide and a structural change from the monoclinic *C*2*c* (HS phase) to the monoclinic $P2_1/c$ (HS-LS phase).[38]

Finally, it is worth noting that the strong cooperativity of the ST shown by the title compounds strongly contrasts with the poorly cooperative SCO behaviors typically observed for other 2D SCO-CP $[Fe(L)_2(NCX)_2]\cdot nS$, where L are more flexible ligands like, for example, bpe and 4,4′-azpy. The strongly cooperative character of the ST is most likely due to the rigidness of the 4,4′-bipy, which is comparable with that observed for the $[Fe(btr)_2(NCX)_2]\cdot H_2O$ system. In the latter compounds the larger hysteresis width could be attributed to the combined effect of smaller size and rigidity of the ligand btr.

CONCLUSION

We have demonstrated for the first time that the 2D coordination polymers $[Fe(4,4'\text{-bipy})_2(NCX)_2]$ (X = S, Se) undergo cooperative SCO behavior when containing an appropriate solvent, in this case 4 mol equiv of chloroform. These SCO behaviors are rare examples of two-step (X = S) and half (X = Se) ST with concomitant crystal phase transition. The intermediate phase is characterized by the presence of an ordered checkerboard-like arrangement of LS and HS states. As in related $[Fe(L)_2(NCX)_2]\cdot nS$ systems, the SCO dramatically depends on the presence or absence of the solvent molecules. The included $CHCl_3$ molecules are not firmly attached and are quite labile, their loss giving a paramagnetic unsolvated species.

EXPERIMENTAL SECTION

$FeSO_4\cdot 7H_2O$, potassium thiocyanate, potassium selenocyante, and 4,4′-bipyridine were all purchased commercially and used as received.

Solvated crystals were grown by the following method, performed in 35 mL screw-top vials: 4,4′-bipy (0.32 g, 2 mmol) was dissolved in 15 mL of chloroform and layered below a filtered $1Fe(II):2NCX^-$ solution formed in an argon atmosphere from $FeSO_4\cdot 7H_2O$ (0.2585 g, 0.93 mmol) and KNCX (1.86 mmol) in 10 mL of methanol. The lower solution was cooled by placing the vial in ice before layering, and a layer of the top solvent (containing no solutes) was placed between the layers before the top layer was added to prevent instant precipitation of powder. After a few days this yielded orange crystals of solvated **1** or **2** at the interface between layers. The chemical composition of the crystals was determined from single crystal X-ray diffraction analyses. Furthermore, the chloroform content was also estimated from the residual solid **1** or **2** after complete desolvation of **1·4CHCl₃** and **2·4CHCl₃**. Yield about 50%.

Crystallography. Single crystal X-ray data were collected on a Bruker APEX diffractometer using Mo−K_α X-radiation. Apart from the IS (120 K) structure of **1**, the structures were all corrected for twinning using the program CellNow, and corrected for absorption using TwinAbs. Crystal structures were solved and refined against all F^2 values using the SHELXTL suite of programs.[39] Non-hydrogen atoms were refined anisotropically, and hydrogen atoms were placed in calculated positions refined using idealized geometries (riding model) and assigned fixed isotropic displacement parameters. Crystallographic details are contained in Table 1.

Magnetic Measurements. Variable-temperature magnetic susceptibility measurements were carried out on microcrystalline samples using a Quantum Design MPMS2 SQUID susceptometer equipped with a 55 kG magnet operating at 1 T in the interval 1.8−300 K. The susceptometer was calibrated with $(NH_4)_2Mn(SO_4)_2\cdot 12H_2O$. Experimental susceptibilities were corrected for diamagnetism of the constituent atoms by the use of Pascal's constants.

Calorimetric Measurements. Differential scanning calorimetry (DSC) measurements were performed on dry samples of $2\cdot 4CHCl_3$ using a Mettler Toledo DSC 821e DSC calorimeter. Low temperatures were obtained with an aluminum block which was attached to the sample holder, refrigerated with a flow of liquid nitrogen, and stabilized at a temperature of 110 K. The sample holder was kept in a drybox under a flow of dry nitrogen gas to avoid water condensation. The measurements

were carried out using around 25−35 mg of powdered and/or single crystal samples sealed in aluminum pans with a mechanical crimp. Temperature and heat flow calibrations were made with standard samples of indium by using its melting (429.6 K, 28.45 J g^{-1}) transition. An overall accuracy of 0.2 K in the temperature and 2% in the heat capacity is estimated. The uncertainty increases for the determination of the anomalous enthalpy and entropy because of the subtraction of an unknown baseline.

■ ASSOCIATED CONTENT

Supporting Information. CIF data for compounds **1·4CHCl$_3$** (120 K), **2·4CHCl$_3$** (100 and 200 K). Derivative of the high-temperature ST of **1·4CHCl$_3$** and magnetic properties of **1** and **2**. This material is available free of charge via the Internet at http://pubs.acs.org.

■ AUTHOR INFORMATION

Corresponding Author
*E-mail: chcja@bris.ac.uk (C.J.A.), jose.a.real@uv.es (J.A.R.).

■ ACKNOWLEDGMENT

This work was supported by the Spanish Ministerio de Ciencia e Innovación (MICINN) and FEDER funds (CTQ2010-18414).

■ REFERENCES

(1) See for example: (a) Goodwin, H. A. *Coord. Chem. Rev.* **1976**, *18*, 293. (b) Gütlich, P. *Struct. Bonding (Berlin)* **1981**, *44*, 83. (c) König, E.; Ritter, G.; Kulshreshtha, S. K. *Chem. Rev.* **1985**, *85*, 219. (d) Hauser, A. *Comments Inorg. Chem.* **1995**, *17*, 17. (e) König, E. *Struct. Bonding (Berlin)* **1991**, *76*, 51. (f) Gütlich, P.; Hauser, A.; Spiering, H. *Angew. Chem., Int. Ed. Engl.* **1994**, *33*, 2024. (g) Sato, O. *Acc. Chem. Res.* **2003**, *36*, 692. (h) Bousseksou, A.; Molnár, G.; Matouzenko, G. *Eur. J. Inorg. Chem.* **2004**, 4353. (i) Real, J. A.; Gaspar, A. B.; Niel, V.; Muñoz, M. C. *Coord. Chem. Rev.* **2003**, *236*, 121. (j) Gütlich, P., Goodwin, H. A., Eds.; *Top. Curr. Chem.* **2004**, Vols. *233*−*235*; (k) Real, J. A.; Gaspar, A. B.; Muñoz, M. C. *Dalton Trans.* **2005**, 2062. (l) Halcrow, M. A. *Polyhedron* **2007**, *26*, 3523. (m) Halcrow, M. A. *Coord. Chem. Rev.* **2009**, *253*, 2493. Olguin, J.; Brooker, S. *Coord. Chem. Rev.* **2011**, *255*, 203. (n) Bousseksou, A.; Molnár, G.; Salmon, L.; Nicolazzi, W. *Chem. Soc. Rev.* **2011**, *40*, 3313.

(2) (a) Freysz, E.; Montant, S.; Lètard, S.; Létard, J.-F. *Chem. Phys. Lett.* **2004**, *394*, 318. (b) Bonhommeau, S.; Molnár, G.; Galet, A.; Zwick, A.; Real, J. A.; McGarvey, J. J.; Bousseksou, A. *Angew. Chem., Int. Ed.* **2005**, *44*, 4069. (c) Cobo, S.; Ostrovskii, D.; Bonhommeau, S.; Vendier, L.; Molnár, G.; Salmon, L.; Tanaka, K.; Bousseksou, A. *J. Am. Chem. Soc.* **2009**, *130*, 9019. (d) Ohba, M.; Yoneda, K.; Agustí, G.; Muñoz, M. C.; Gaspar, A. B.; Real, J. A.; Yamasaki, M.; Ando, H.; Nakao, Y.; Sakaki, S.; Kitagawa, S. *Angew. Chem., Int. Ed.* **2009**, *48*, 4767.

(3) (a) Haasnoot, J. G.; Vos, G.; Groeneveld, W. L. *Z. Naturforsch., Teil B* **1977**, *32*, 1421. (b) Michalowicz, A.; Moscovici, J.; Ducourant, B.; Craco, D.; Kahn, O. *Chem. Mater.* **1995**, *7*, 1833.

(4) (a) Lavrenova, L. G.; Ikorski, V. N.; Varnek, V. A.; Oglezneva, I. M.; Larionov, S. V. *Koord. Khim.* **1986**, *12*, 207. (b) Lavrenova, L. G.; Ikorski, V. N.; Varnek, V. A.; Oglezneva, I. M.; Larionov, S. V. *Koord. Khim.* **1986**, *12*, 207. (c) Lavrenova, L. G.; Ikorski, V. N.; Varnek, V. A.; Berezovskii, G. A.; Bessergenev, V. G.; Bausk, N. V.; Eremburg, S. B.; Larionov, S. V. *Koord. Khim.* **1996**, *22*, 357. (d) Kröber, J.; Audière, R.; Claude, R.; Codjovi, E.; Kahn, O.; Haasnoot, J. G.; Crolière, F.; Jay, C.; Bousseksou, A.; Linares, J.; Varret, F.; Gonthier-Vassal, A. *Chem. Mater.* **1994**, *6*, 1404. (e) Garcia, Y.; van Koningsbruggen, P. J.; Lapouyade, P.; Rabardel, L.; Kahn, O.; Wierczorek, M.; Bronisz, R.; Ciunik, Z.; Rudolf, M. F. *C. R. Acad, Sci. Paris IIc* **1998**, *1*, 523.

(5) (a) Bronisz, R. *Inorg. Chem.* **2005**, *44*, 4463. (b) Garcia, Y.; Kahn, O.; Rabardel, L.; Chansou, B.; Salmon, L.; Tuchagues, J. P. *Inorg. Chem.* **1999**, *38*, 4663. (c) Gu, Z. G.; Xu, Y. F.; Zhou, X. H.; Zuo, J. L.; You, X. Z. *Cryst. Growth Des.* **2008**, *8*, 1306. (d) Roubeau, O.; Haasnoot, J. G.; Codjovi, E.; Varret, F.; Reedijk, J. *Chem. Mater.* **2002**, *14*, 2559. (e) Roubeau, O.; Gomez, J. M. A.; Balskus, E.; Kolnaar, J. J. A.; Haasnoot, J. G.; Reedijk, J. *New. J. Chem.* **2001**, *25*, 144.

(6) (a) van Koningsbruggen, P. J.; Garcia, Y.; Kahn, O.; Fournès, L.; Kooijman, H.; Haasnoot, J. G.; Moscovici, J.; Provost, K.; Michalowicz, A.; Renz, F.; Gütlich, P. *Inorg. Chem.* **2000**, *39*, 891. (b) Schweifer, J.; Weinberger, P.; Mereiter, K.; Boca, M.; Reichl, C.; Wiesinger, G.; Hilscher, G.; van Koningsbruggen, P. J.; Kooijman, H.; Grunert, M.; Linert, W. *Inorg. Chim. Acta* **2002**, *339*, 297. (c) van Koningsbruggen, P. J.; Garcia, Y.; Kooijman, H.; Spek, A. L.; Haasnoot, J. G.; Kahn, O.; Linares, J.; Codjovi, E.; Varret, F. *J. Chem. Soc., Dalton Trans.* **2001**, 466. (d) Grunert, C. M.; Schweifer, J.; Weinberger, P.; Linert, W.; Mereiter, K.; Hilscher, G.; Müller, M.; Wiesinger, G.; van Koningsbruggen, P. J. *Inorg. Chem.* **2004**, *43*, 155. (e) Bronisz, R. *Inorg. Chem.* **2007**, *46*, 6733. (f) Bialonska, A.; Bronisz, R.; Weselski, M. *Inorg. Chem.* **2008**, *47*, 4436. (g) Quesada, M.; Kooijman, H.; Gamez, P.; Costa, J. S.; van Koningsbruggen, P. J.; Weinberger, P.; Reissner, M.; Spek, A. L.; Haasnoot, J. G.; Reedijk, J. *Dalton Trans.* **2007**, 5434. (h) van Koningsbruggen, P. J.; Garcia, Y.; Kooijman, H.; Spek, A. L.; Haasnoot, J. G.; Kahn, O.; Linares, J.; Codjovi, E.; Varret, F. *J. Chem. Soc., Dalton Trans.* **2001**, 466.

(7) (a) Quesada, M.; Peña-O'Shea, V. A.; Aromí, G.; Geremia, S.; Massera, C.; Roubeau, O.; Gamez, P.; Reedijk, J. *Adv. Mater.* **2007**, *19*, 1397. (b) Bao, X.; Liu, J.-L.; Leng, J.-D.; Lin, Z.; Tong, M.-L.; Nihei, M.; Oshio, H. *Chem.—Eur. J.* **2010**, *16*, 7973. (c) Neville, S. M.; Leita, B. A.; Offermann, D. A.; Duriska, M. B.; Moubaraki, B.; Chapman, K. W.; Halder, G. J.; Murray, K. S. *Eur. J. Inorg. Chem.* **2007**, 1073.

(8) (a) Kitazawa, T.; Gomi, Y.; Takahashi, M.; Takeda, M.; Enomoto, M.; Miyazaki, A.; Enoki, T. *J. Mater. Chem.* **1996**, 6. (b) Niel, V.; Martínez-Agudo, J. M.; Muñoz, M. C.; Gaspar, A. B.; Real, J. A. *Inorg. Chem.* **2001**, *40*, 3838. (c) Niel, V.; Thompson, A. L.; Muñoz, M. C.; Galet, A.; Goeta, A. E.; Real, J. A. *Angew. Chem., Int. Ed.* **2003**, *42*, 3760. (d) Niel, V.; Thompson, A. L.; Goeta, A. E.; Enachescu, C.; Hauser, A.; Galet, A.; Muñoz, M. C.; Real, J. A. *Chem.—Eur. J.* **2005**, *11*, 2047. (e) Galet, A.; Niel, V.; Muñoz, M. C.; Real, J. A. *J. Am. Chem. Soc.* **2003**, *125*, 14224. (f) Kosaka, W.; Nomura, K.; Hashimoto, K.; Ohkoshi, S. *J. Am. Chem. Soc.* **2005**, *127*, 8590. (g) Arai, M.; Kosaka, W.; Matsuda, T.; Ohkoshi, S. *Angew. Chem.* **2008**, *120*, 6991. (h) Muñoz, M. C.; Real, J. A. *Coord. Chem. Rev.* **2011**, *255*, 2068.

(9) Genre, C.; Jeanneau, E.; Bousseksou, A.; Luneau, D.; Borshch, S. A.; Matouzenko, G. S. *Chem.—Eur. J.* **2008**, *14*, 697.

(10) Dupouy, G.; Marchivie, M.; Triki, S.; Sala-Pala, J.; Gómez-García, C. J.; Pillet, S.; Lecomte, C.; Létard, J.-F. *Chem. Commun.* **2009**, 3404.

(11) Vreugdenhil, W.; Van Diemen, J. H.; De Graaff, R. A. G.; Haasnoot, J. G.; Reedijk, J.; Van Der Kraan, A. M.; Kahn, O.; Zarembowitch, J. *Polyhedron* **1990**, *9*, 2971.

(12) Ozarowski, A.; Shunzhong, Y.; McGarvey, B. R.; Mislankar, A.; Drake, J. E. *Inorg. Chem.* **1991**, *30*, 3167.

(13) Moliner, N.; Muñoz, M. C.; Létard, S.; Solans, X.; Menéndez, N.; Goujon, A.; Varret, F.; Real, J. A. *Inorg. Chem.* **2000**, *39*, 5390.

(14) Real, J. A.; Andrés, E.; Muñoz, M. C.; Julve, M.; Granier, T.; Bousseksou, A.; Varret, F. *Science* **1995**, *268*, 265.

(15) Neville, S. M.; Halder, G. J.; Chapman, K. W.; Duriska, M. B.; Moubaraki, B.; Murray, K. S.; Kepert, C. J. *J. Am. Chem. Soc.* **2009**, *131*, 12106.

(16) Neville, S. M.; Moubaraki, B.; Murray, K. S.; Kepert, C. J. *Angew. Chem., Int. Ed.* **2007**, *46*, 2059.

(17) Halder, G. J.; Kepert, C. J. *Aust. J. Chem.* **2005**, *58*, 311.

(18) Halder, G. J.; Kepert, C. J.; Moubaraki, B.; Murray, K. S.; Cashion, J. D. *Science* **2002**, *298*, 1762.

(19) Adams, C. J.; Real, J. A.; Waddington, R. E. *CrystEngComm* **2010**, *12*, 3547.

(20) Slichter, C. P.; Drickamer, H. G. *J. Chem. Phys.* **1972**, *56*, 2142.

(21) Sorai, M.; Nakano, M.; Miyazaki, Y. *Chem. Rev.* **2006**, *106*, 976.

(22) (a) Martin, J. P.; Zarembowifch, J.; Bousseksou, A.; Dworkin, A.; Haasnoot, J. G.; Varret, F. *Inorg. Chem.* **1994**, *33*, 6325. (b) Martin,

J. P.; Zarembowifch, J.; Dworkin, A.; Haasnoot, J. G.; Codjovi, E. *Inorg. Chem.* **1994**, *33*, 2617.
(23) Verat, A. Y.; Ould-Moussa, N.; Jeanneau, E.; Le Guennic, B.; Bousseksou, A.; Borshch, S. A.; Matouzenko, G. S. *Chem.—Eur. J.* **2009**, *15*, 10070.
(24) Fedaoui, D.; Bouhadja, Y.; Kaiba, A.; Guionneau, P.; Létard, J. F.; Rosa, P. *Eur. J. Inorg. Chem.* **2008**, 1022.
(25) Moliner, N.; Muñoz, M. C.; Létard, S.; Salmon, L.; Tuchagues, J. P.; Bousseksou, A.; Real, J. A. *Inorg. Chem.* **2002**, *41*, 6997.
(26) (a) Matouzenko, G. S.; Molnar, G.; Bréfuel, N.; Perrin, M.; Bousseksou, A.; Borshch, S. A. *Chem. Mater.* **2003**, *15*, 550. (b) Genre, C.; Matouzenko, G. S.; Jeanneau, E.; Luneau, D. *New J. Chem.* **2006**, *30*, 1669.
(27) Weber, B.; Tandon, R.; Himsl, D. *Z. Anorg. Allg. Chem.* **2007**, *633*, 1159.
(28) Yoneda, K.; Adachi, K.; Hayami, S.; Maeda, Y.; Katada, M.; Fuyuhiro, A.; Kawata, S.; Kaizaki, S. *Chem. Commun.* **2006**, 45.
(29) Niel, V.; Muñoz, M. C.; Gaspar, A. B.; Galet, A.; Levchenko, G.; Real, J. A. *Chem.—Eur. J.* **2002**, *8*, 2446.
(30) Wriedt, M.; Sellmer, S.; Näther, C. *Dalton Trans.* **2009**, 7975.
(31) Zhang, Y.; Jianmin, L.; Nishiura, M.; Imamoto, T. *J. Mol. Struct.* **2000**, *519*, 219.
(32) (a) Guionneau, P.; Marchivie, M.; Bravic, G.; Létard, J. F.; Chasseau, D. *Top. Curr. Chem.* **2004**, *234*, 97. (b) Hazen, R. M.; Finger, L. W. *Comparative Crystal Chemistry. Temperature, Pressure, Composition and the Variation of Crystal Structure*; John Wiley & Sons Ltd: New York, 1984.
(33) Garcia, J.; Bravic, G.; Gieck, C.; Chasseau, D.; Tremel, W.; Gütlich, P. *Inorg. Chem.* **2005**, *44*, 9723.
(34) Neville, S. M.; Halder, G. J.; Chapman, K. W.; Duriska, M. B.; Southon, P. D.; Cashion, J. D.; Létard, J. F.; Moubaraki, B.; Murray, K. S.; Kepert, C. J. *J. Am. Chem. Soc.* **2008**, *130*, 2869.
(35) Martínez, V.; Gaspar, A. B.; Muñoz, M. C.; Bukin, G. V.; Levchenko, G.; Real, J. A. *Chem.—Eur. J.* **2009**, *15*, 10960.
(36) Halder, G. J.; Chapman, K. W.; Neville, S. M.; Moubaraki, B.; Murray, K. S.; Létard, J. F.; Kepert, C. J. *J. Am. Chem. Soc.* **2008**, *130*, 17552.
(37) Agustí, G.; Muñoz, M. C.; Gaspar, A. B.; Real, J. A. *Inorg. Chem.* **2008**, *47*, 2552.
(38) Agustí, G.; Gaspar, A. B.; Muñoz, M. C.; Real, J. A. *Inorg. Chem.* **2007**, *46*, 9646.
(39) Sheldrick, G. M. *Acta Crystallogr.* **2008**, *A64*, 112.